Acta Materialia 118 (2016) 177–186

Contents lists available at ScienceDirect

Acta Materialia

journal homepage: www.elsevier.com/locate/actamat

Full length article

Atomic-scale segregations at the deformation-induced symmetrical boundary in an Mg-Zn-Y alloy

X.H. Shao [a], Z.Z. Peng [a], Q.Q. Jin [a, b], X.L. Ma [a, *]

[a] Shenyang National Laboratory for Materials Science, Institute of Metal Research, Chinese Academy of Sciences, Shenyang 110016, China
[b] School of Materials Science and Technology, University of Science and Technology of China, Hefei 230026, China

ARTICLE INFO

Article history:
Received 20 May 2016
Received in revised form
26 July 2016
Accepted 27 July 2016

Keywords:
Mg alloy
LPSO phases
Solute segregation
Deformation kink
Deformation twin

ABSTRACT

Solute atoms segregation to the interfaces, such as grain boundary or twin boundary, often plays a critical role in modulating the properties of a metallic alloy. Deformation induced segregation to the interfaces has been a subject of significant research, since this is one of the key issues to fully understand the deformation mechanism and microstructure evolution in service of engineering materials. By means of the high-resolution aberration-corrected scanning transmission electron microscopy (STEM), we report the investigations of segregations to symmetrical boundaries, kink boundary (KB) and twin boundary (TB), in the Mg-Zn-Y alloys containing long period stacking ordered (LPSO) phases subjected to a compression at room temperature. We found that Zn atoms preferentially segregate to the deformation-induced symmetrical KBs in the LPSO structures and sandwiched Mg layers, while only a small amount of Y atoms concentrate at KB in LPSO structure. These enriched atoms may be in a random distribution, form nanoscale clusters or in a periodic pattern. Furthermore, solute atoms would rather decorate the segment of coherent TBs than enrich the overlapped TBs. Based on the direct atomic observations, the segregation mechanisms to the featured microstructures are proposed.

1. Introduction

Owing to the good mechanical properties, magnesium-transition metal (TM)-rare earth (RE) alloys containing long-period stacking ordered (LPSO) phase have received considerable attentions [1–5]. The volume fraction, orientation and distribution of the LPSO structure in an Mg alloy play a significant role in modulating the mechanical performance [6–8]. Extensive effort has been made to understand the deformation mechanism of this kind of Mg alloys [4–7,9–14]. Deformation kink in the LPSO structure is one of the major deformation mechanisms responsible for the high strength and good ductility both at room temperature and high temperatures of the Mg alloys [5–7,9,10,14,15]. The origin of deformation kink in the LPSO phase is known to result from the synchronized slip of basal dislocations [5], and it has also been reported to originate from a progressive rotation of the lattice by avalanche generation of pairs of dislocations on the basal plane [7]. Deformation twinning, another important deformation mode in these Mg alloys, might be suppressed by strong interaction with LPSO structures or SFs enriched with Zn/Y atoms [5,9,13].

Segregation of solute atoms in Mg alloys to interfaces, e. g., grain boundary (GB) and twin boundary (TB), during deformation also has a significant impact on their mechanical properties. For example, Gd atoms or clusters were found to segregate to GBs in the Mg-Gd alloys after cold rolling and aging or hot extrusion, which is beneficial to the weakening of the basal texture of the Mg alloys [16,17]. Gd and Zn atoms were observed to periodically decorate the coherent TBs in the dilute Mg-Gd/Zn alloys after deformation and annealing, pinning the TB and subsequent strengthening the materials [18]. Zn/Y atoms also tend to concentrate at stacking faults in the Mg-Zn-Y alloys during hot deformation [19]. The interfaces segregation is usually reported to play a critical role in tailoring the mechanical performance of materials. The GB segregation can either strengthen the materials by lowering the movement of GBs [20], stabilizing the nanometer materials [21], and improving the ductility [22], or weaken the materials via GB brittleness [23]. However, there is little knowledge about the segregation of solute atoms at the deformation-induced interfaces, kink boundaries (KBs) and twin boundaries (TBs), in the Mg-Zn-Y alloys with the LPSO structures. The recent developed aberration-corrected

* Corresponding author.
E-mail address: xlma@imr.ac.cn (X.L. Ma).

http://dx.doi.org/10.1016/j.actamat.2016.07.054
1359-6454/

scanning transmission electron microscopy (STEM) enables us to acquire the microstructure and chemical feature of the interfaces at the atomic-scale [16,18,24,25].

It is the purpose of this study to apply the aberration-corrected STEM technique to investigate the segregation of Zn/Y atoms at the deformation-induced KB and TB of an Mg-Zn-Y alloy. We unraveled the distribution and chemical features of solute atoms which segregated along KB in LPSO structures and sandwiched Mg layers. We also characterized the microstructure of TBs that interacted with SFs enriched with Zn/Y. Based on the direct observations, the segregation mechanism is discussed and a physical model is then proposed. This result may provide new insights into the boundary segregation of Mg alloys during deformation at room temperature.

2. Experimental procedure

The casting procedure of the $Mg_{97}Zn_1Y_2$ (at.%) alloy is described in Ref. [5]. Specimens with the dimensions Φ 4 × 8 mm^3 were cut from the ingots by electrical discharge machining, and the compression direction was parallel to the long axis of the specimens. The compression experiments were carried out at room temperature and a strain rate of 1.0×10^{-3} s^{-1} in a Gleeble-1500 thermal simulation machine. Transmission electron microscopy (TEM) samples parallel to the compression direction were sliced by a linear precision saw. The samples were then ground using variant grit silicon carbide papers, and finally ion milled by Gatan 691 precision ion polishing system. Fine ion milling was done at 4 keV for 10 min, 3 keV for approximately 20 min and then 1 keV for 20 min, with an incident angle of 4.5°, in order to largely reduce the thermal effect of ion milling on the structure of TEM samples [26,27]. The voltage and incident angle used here are much lower than the typical condition, thus one can expect that the temperature rise of the TEM samples should be efficiently minimized and its effect could be negligible. The microstructural and chemical investigations were performed parallel to the compression axis. Atomic-resolution high-angle annular dark field (HAADF) observation was conducted on an aberration-corrected scanning transmission electron microscope (STEM) operated at 300 kV, FEI Titan^{3}™ G^2 60–300 TEM. The probe convergence is 25 mrad which yields a probe size of less than 0.1 nm. And associated energy dispersive X-ray spectroscopy (EDS) is employed to analyze the chemical features of interfaces in the Mg-Zn-Y alloys. The EDS spectrum or mapping in this work is carried out with a probe size of approximately 0.3 nm in diameter. Two dimensional (2D) graphs via Matlab display the intensity values of EDS mapping of Mg, Zn and Y elements, in order to further demonstrate the distribution of the solute atoms.

3. Experimental results

3.1. Microstructural characteristics of the $Mg_{97}Zn_1Y_2$ alloy before deformation

The typical SEM microstructure of the $Mg_{97}Zn_1Y_2$ alloy is shown in Fig. 1a. The LPSO structures exhibit brighter contrast due to the enrichment of Zn/Y atoms, while the matrix shows darker contrast. The LPSO structures with a width of hundreds to thousands of nanometers are usually present in the form of a strong sketch, which play a significant role in improving the mechanical properties of the $Mg_{97}Zn_1Y_2$ alloy [5]. Meanwhile, profuse stacking faults (SFs) enriched with Zn/Y atoms or lamellar LPSO structures in the matrix are parallel to the basal plane of Mg, as shown in Fig. 1b. These planar structures probably block the propagation of deformation twin due to the strong interaction between SFs and twins in Mg alloys [13]. The LPSO phases and SFs in as-cast Mg-Zn-Y alloys are thoroughly documented to contain AB'C'A building block, where the Zn/Y are enriched in the B′ and C′ planes [28–30] and Y atoms are recently proved to be also in A planes in Mg-Zn-Y alloys [31,32] and Mg-Al-Gd alloys [33,34]. We performed an EDS analysis with the sub-nanometer probe and figured out the chemical nature of the LPSO structure and SFs, as shown with the inset in Fig. 1b. The line profile demonstrates that both Zn and Y are remarkably enriched at the B′ and C′ layers. In particular, the quantity of Y atoms is more than that of Zn in AB'C'A blocks, which is consistent with the results reported in RS P/M $Mg_{97}Y_2Zn_1$ alloys [28,35]. It is worthwhile to mention that the SFs in this work especially represent the SFs enriched with Zn/Y atoms, which are similar to γ′ phase formed after ageing for a long time in Mg-RE-Zn alloys [36,37] as far as the stacking sequence and solute atoms segregation are taken into account.

3.2. Deformation kink in the LPSO structure/SFs and Mg layers

Deformation kink is one of the major deformation mechanisms for the LPSO structures in Mg-Zn-Y alloys [4,5,7]. As shown in Fig. 2a, the optical micrograph shows that the compression-induced deformation kinks in the LPSO structures range from 1 to 5 μm in width, and in the meanwhile kinks also occur in the neighboring Mg matrix, marked by upward and backward arrows, respectively. The low magnification HAADF-STEM image, as seen in Fig. 2b, further demonstrates the multiple nano-scaled kinks penetrate the LPSO structures, SFs and the sandwiched Mg layers. This observation is in accordance with the kink produced upon compression at 573 K [5]. It proves that the deformation kink in the LPSO structures could propagate into Mg interlayers and neighboring Mg grains at various deformation temperatures. M. Yamasaki et al. reported that three kinds of deformation kinks could be produced during deformation, <1$\bar{2}$10>, <0001>, <1$\bar{1}$00> and <0$\bar{1}$10> rotation-type kink [38]. In this work, we focused on investigating the solute segregation of <1$\bar{2}$10> rotation-type symmetrical deformation kink by using atomic-resolution HAADF-STEM.

Fig. 3a shows a low magnification STEM image of a symmetrical deformation kink in LPSO structures and the sandwiched Mg layers, recorded along [11$\bar{2}$0] zone axis of Mg. The misorientation of basal planes of the deformation kink is about 78°. It is well known that the HAADF-STEM technique provides atomic number (Z) contrast with the intensity in proportion to $Z^{1.7-1.9}$ [39,40]. The brighter contrast along KB thus implies that heavier atoms segregate at KB both in LPSO phase and Mg interlayers during deformation. The high resolution STEM images of KB, framed by rectangles *b*, *c* and *d* in Fig. 3a are displayed in Fig. 3b–d. Apparently, heavier atoms segregate to the KB in the LPSO phase, as denoted by arrows in Fig. 3b. This scenario is more obvious in the interface of LPSO and Mg layers, as shown in Fig. 3c. The heavier atoms segregate at the KB in the Mg-enriched planes but are deficient in the Zn/Y-enriched planes of LPSO structures, marked by solid and open arrows in Fig. 3c, respectively. Likewise, the heavier atoms are in a random distribution at KB in sandwiched Mg layer of 6 nm (Fig. 3c) and that of 100 nm in thickness (Fig. 3d). Nie et al. has in fact demonstrated that analogous symmetrical KBs with other misorientation angles in LPSO structure of Mg-Zn-Y alloy exhibit brighter contrast [41]. This strongly implies that the solute atoms tend to be enriched in the KB during deformation.

The solute atoms along the KB are also present in the form of nanoscale clusters or in a periodic pattern in the samples natural annealing for 10 months, as shown in Fig. 4. The symmetrical KBs exhibit bright contrast in the low magnification STEM images, Fig. 4a–c, suggesting that the KBs are rich of heavier atoms. Fig. 4b is a high magnification of KB marked with *b* in Fig. 4a, demonstrates

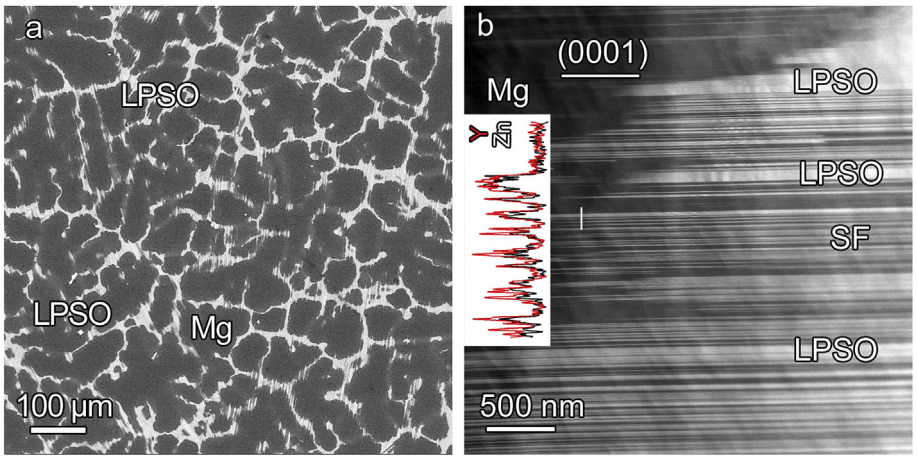

Fig. 1. (a) A low magnification SEM image showing the microstructural characteristics of the Mg-Zn-Y alloy before compression. The area in brighter contrast is basically composed of LPSO and SFs, while the darker areas correspond to Mg matrix. (b) The basal plane of the LPSO structures is parallel to that of Mg matrix; The SFs also occur in the basal planes.

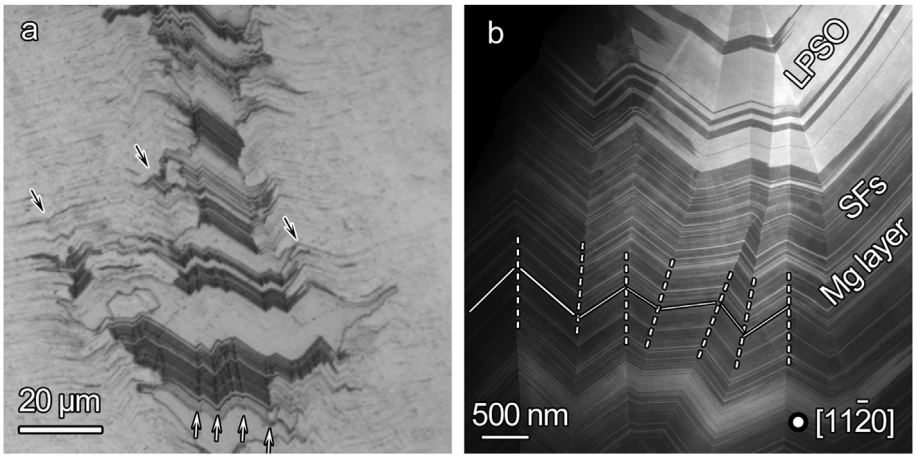

Fig. 2. (a) Optical micrograph showing the features of the Mg-Zn-Y alloy compressed at room temperature. The deformation kinks in the LPSO phase are marked with upward arrows; while the kinks in the Mg matrix are indicated with downward arrows. (b) An HAADF-STEM image showing the multiple kinks in the LPSO structures, in SFs and in the sandwiched Mg layers. The basal planes of the Mg layers are denoted with the solid lines, and KBs are marked with the dotted lines.

that 4–8 heavier atoms tend to form a nanocluster in the Mg layers, recorded along [11$\bar{2}$0] direction. However, the segregation of atoms possibly blur the microstructure of KB in the SFs, as denoted by the arrow. Moreover, the heavier atoms may periodically decorate the 60° KB of Mg layers sandwiched in the lamellar LPSO structures, as illustrated in Fig. 4d. The periodic bright dots distributing along KB represents the columns enriched with Zn/Y. Interestingly, this case is the same as the microstructural feature of the periodic segregation of Gd/Zn atoms in {10$\bar{1}$ 1} TB [18]. Note that the {10$\bar{1}$ 1} twin angle of Mg is 61.9°. Therefore, the solute atoms tend to segregate at special sites along the symmetrical TB or KB of approximately 60°. This unique microstructure of the produced boundaries would minimize strain energy and even the total system energy [18]. Thus solute atoms prefer to segregate to the deformation-induced KB, irrespective of the misorientation angle. The difference is the various configuration of solute atoms along local KB, which should be intimately related to the local KB's microstructure.

3.3. Chemical feature of kink boundary in LPSO structures and SFs

To identify the solute atoms, we carried out the EDS analysis on the symmetrical KB along [11$\bar{2}$0] zone axis. Fig. 5a shows a typical deformation KB in LPSO structures and Mg layers. The EDS mapping demonstrates the segregation of Zn at the KB both in LPSO structures and in the sandwiched Mg layers, as illustrated in Fig. 5b, but the contrast of Y atoms along KB cannot be clearly discerned. The diameter of segregation is approximately 2 nm at KB. The intensity values of Fig. 5b were further displayed in 2D graphs via Matlab, as shown in Fig. 5c. It certifies that no obvious concentration gradient of solute atoms was detectable from the KB to the LPSO structures laterally in basal planes. Specifically, a small amount of Y atoms are proved to be enriched at KB in LPSO structure but no Y atoms concentrate at KB in Mg layers, denoted by solid and open arrows in Fig. 5c, respectively. Fig. 6 shows the segregation feature along the KB in the intergrowth microstructure of SFs and Mg layers, which is analogous to the phenomenon along KB in the LPSO structures and Mg layers. Zn atoms apparently aggregated to the KB in the SFs and Mg layers, with about 2 nm in width, presented in Fig. 6b. No obvious Y atoms segregated to the KB even at the intersection of KB and the SFs, denoted by solid arrow in Fig. 6c. This is a little different from the concentration of Y atoms at KB of LPSO structures.

We further surveyed solute atoms spectra at the center of KB and the neighboring region in LPSO structure or SFs, about 10 nm departing from the KB, denoted by white and yellow arrow in Figs. 5b and 6b. The amount of solute atoms is listed in Table 1. Here,

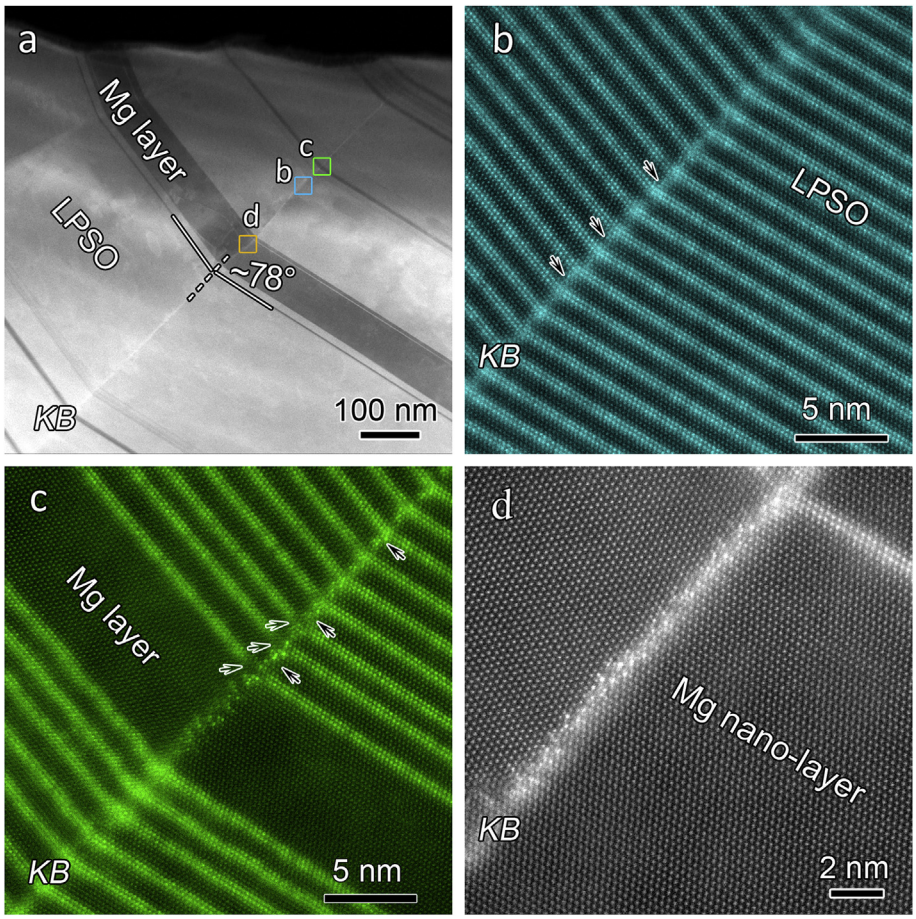

Fig. 3. (a) A low magnification HAADF-STEM image showing the kink bands in the LPSO structures and Mg layers. Note that the KBs exhibit bright contrast. (b–d) High magnification STEM images corresponding to the areas framed with "b", "c", "d", respectively, in (a). Note that all of the KBs in LPSO and Mg layers display brighter contrast, implying that the KBs are decorated with heavier atoms.

$\delta^{Zn}_{KB-LPSO}$, $\delta^{Y}_{KB-LPSO}$, δ^{Zn}_{LPSO}, δ^{Y}_{LPSO}, δ^{Zn}_{KB-SF}, and δ^{Zn}_{SF} are introduced to represent the amount of Zn and Y atoms at KB or in LPSO/SF near KB. The content of Zn atoms at KB of LPSO structures and that of SFs, about 20.8 ± 4.5 at.% and 8.0 ± 2.1 at.%, respectively, are much higher than the solubility of Zn in Mg matrix (~2.4 at.%). It can be found that $\delta^{Zn}_{KB-LPSO}$ is approximately 3 times of δ^{Zn}_{LPSO}, while $\delta^{Y}_{KB-LPSO}$ is almost the same as δ^{Y}_{LPSO}, where δ^{Zn}_{LPSO} and δ^{Y}_{LPSO} are much the same as those in the original LPSO structures before deformation. By contrast, δ^{Zn}_{KB-SF} is about 2 times of δ^{Zn}_{SF}. The amount of Y atoms detected in SFs or intersection of KB and SFs evaluated is much lower, so it was not included here. It has been reported that the segregation level of solutes at GBs induced by high-pressure torsion varies from one GB to another [42]. This is proposed to be due to the difference in structural characteristics of various GBs, which implies the determination of GBs' structure to the solute segregation. In analogous, the solute level of segregation along the KB of LPSO structures and SFs would be affected by the microstructures of various KBs.

3.4. Solute atoms segregation along partially coherent {10$\bar{1}$ 2} twin boundaries

Fig. 7 shows the microstructural feature of {10$\bar{1}$ 2} TB which interacted with SFs during compression. Fig. 7a and b are the bright TEM image and corresponding STEM image of the deviated {10$\bar{1}$ 2} TB. The image in Fig. 7b is rotated about 35° relative to that in Fig. 7a. By doing so, the SFs in the matrix are vertical. The TB exhibits weak contrast in TEM mode, while shows bright contrast in the STEM mode, as denoted by arrows in Fig. 7b. We carried out EDS mapping to analyze the chemical feature of TB here. As inserted in Fig. 7b, Zn atoms segregated at TB while no obvious Y atoms could be detected in the interested region, framed by a red rectangle. Furthermore, TB crossed over the profuse SFs (the vertical lines in Fig. 7b) without apparent deviation or steps. Fig. 7c–e are the atomic resolution STEM images of the TB marked by a white rectangle in Fig. 7b, indicating Zn atoms periodically segregated into the coherent segments of {10$\bar{1}$ 2} TB. The inset fast flourier transformation (FFT) pattern in Fig. 7c clarified the misorientation angle between the basal plane in matrix and that in twin is about 95.9°. This twin angle deviated from the ideal twin angle of {10$\bar{1}$ 2} twin, e. g. 86.3°, which originated from the strong interaction between dense SFs and deformation twin [13]. The above periodic segregation of Zn/Y atoms does not occur in a particular section of the TB. Note that such a section is within a pair of SFs, 8 nm apart from each other, denoted by the arrow in Fig. 7d. The inset in (d) is a high-resolution STEM image showing a combination of TBs and basal-prismatic (BP) interfaces. The TB consists of {10$\bar{1}$ 2} coherent TBs with Zn/Y segregations and the BP interfaces free of Zn/Y atoms segregations, denoted by red and green circles, respectively. It is worthwhile to note that the configuration of solute atoms in the TB is significantly different from periodic distribution of Gd/Zn in the coherent twin boundaries (CTB) in Mg dilute alloys after aging [18], which may be indicative of metastable state of solute atoms along

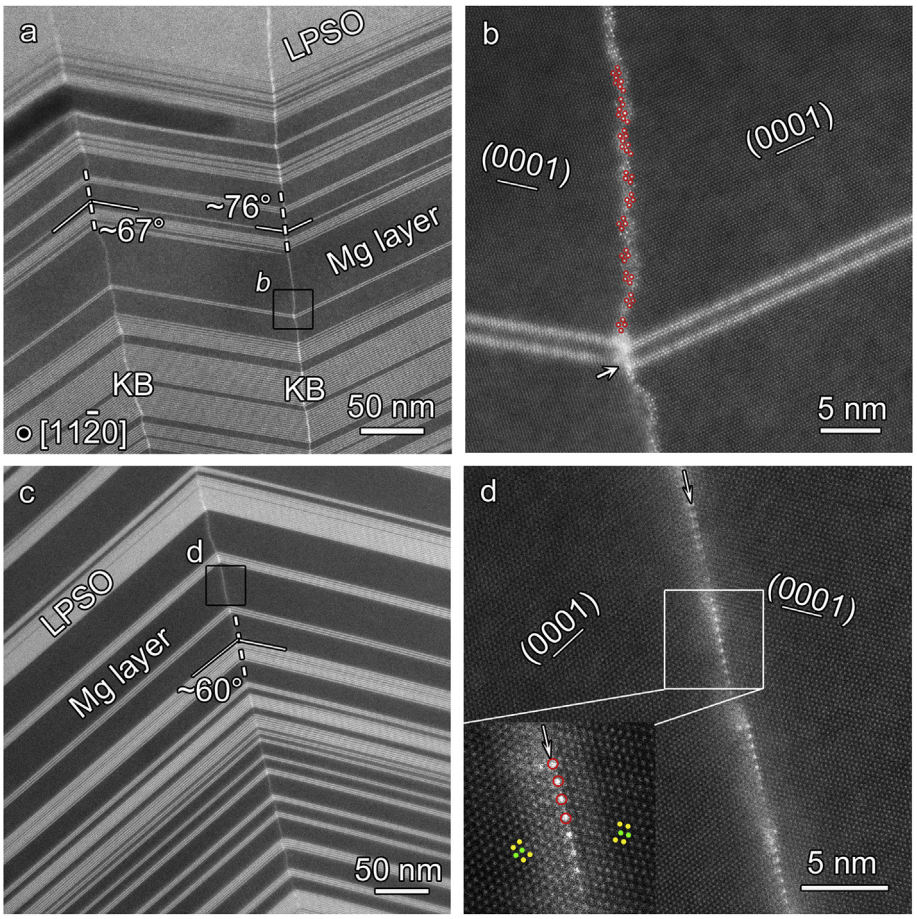

Fig. 4. (a) HAADF-STEM image showing the KBs with brighter contrast in the LPSO structures and in the Mg layers in the samples natural annealed for 10 months. (b) High magnification HAADF-STEM image of the area indicated with "b" in (a). The brighter atoms (namely, the heavier atoms) tend to form clusters along the KBs. (c) HAADF-STEM image showing a KB with brighter contrast in the LPSO structures and in the Mg layers. (d) High magnification HAADF-STEM image of the area indicated with "d" in (c). The brighter atoms preferentially segregate to specific atomic sites along the KB, and the distribution of the solute atoms shows a periodic array.

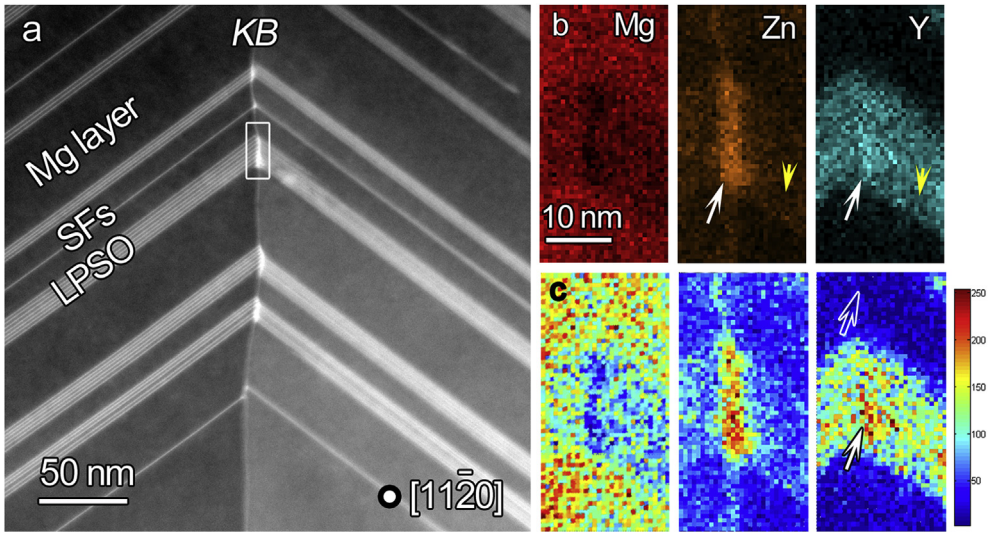

Fig. 5. (a) An HAADF-STEM image of a typical symmetrical KB of LPSO structures and Mg layers; (b) EDS chemical maps corresponding to the framed area in (a), clearly show the segregation of Zn atoms along KB both in LPSO structures and in Mg layers; (c) 2D intensity maps of Mg, Zn and Y elements corresponding to (b) via Matlab, further clarify the Zn segregation along KB. Note that a little bit contrast of Y atoms exhibits along KB in LPSO structures, while no contrast in Mg layers, marked by a solid arrow and an open arrow in (c), respectively.

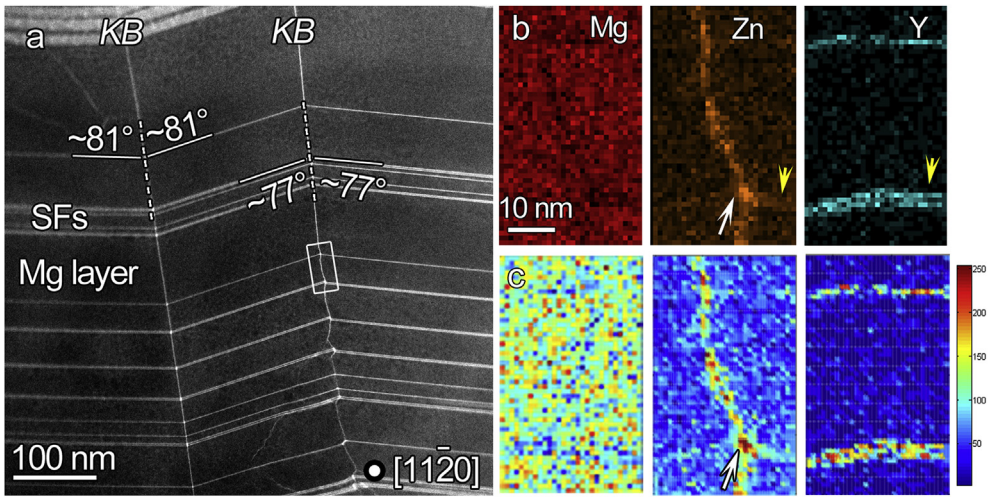

Fig. 6. (a) An HAADF-STEM image of a typical symmetrical KBs in the SFs and Mg layers; (b) EDS chemical maps of the marked region in (a), illustrate the enrichment of Zn along KB both in SFs and Mg layers; (c) 2D intensity maps of Mg, Zn and Y elements corresponding to (b) via Matlab. Compared to the case in Fig. 5, only Zn atoms could be detected along KB both in SFs and in Mg layers.

Table 1
The amounts of Zn and Y atoms at KB or in the vicinity of LPSO structure and in SFs, denoted by a white and yellow arrow, respectively, are evaluated based on the surveying spectra of EDS mapping in Figs. 5 and 6.

	KB & LPSO	LPSO	KB & SF	SF
Zn (at. %)	20.8 ± 4.5	6.5 ± 1.5	8.0 ± 2.1	4.5 ± 0.5
Y (at. %)	8.4 ± 4.4	8.1 ± 2.1	[a]	[a]

[a] No obvious Y could be detected at KB at SFs and also in SFs.

deformation-induced TB. Fig. 7e shows a random distribution of solute atoms along the TB, compared with those along TB in Fig. 7c and d. Such a disorder should be a resultant from the interaction of TB with two units of SFs. This was confirmed by the inserted FFT pattern which shows the local misorientation angle of matrix and twin is up to 102.5°. The large deviation of TB from the {10$\bar{1}$ 2} twin plane has been observed in pure Mg [43] and pure Co [44,45], which is explained based on the dislocation theory. In our case, this is additionally accounted for the interaction between TB and SFs.

3.5. No segregation along overlapped twin boundaries

Fig. 8a is a TEM bright field image of a 200 nm-wide matrix enclosed in a {10$\bar{1}$ 2} deformation twin, and the selected area electron diffraction (SAED) pattern is inserted. A great many black lines shown in Fig. 8a represent profuse SFs enriched with Zn/Y in the DT and matrix [5]. The corresponding low magnification STEM image of the matrix and DT is presented in Fig. 8b, with a small rotation. The weak contrast of the TB may indicate that there is almost no Zn/Y segregation along TB, which is confirmed by atomic resolution STEM images. In addition, the rumpled SFs in matrix and twins are continuous and without large deviation. Fig. 8c and d are the high resolution STEM images of the regions marked by *c* and *d* in Fig. 8b, showing the stacking sequence and chemical distribution of Zn/Y elements in the matrix and at TB. Fig. 8c indicates that solute atoms didn't segregate along {10$\bar{1}$ 2} overlapped TBs between SFs, about 10 nm in length. The overlapped TB presented here is indeed not sharp at the atomic level due to interaction between SFs with deformation twin [13], which is slightly different from the fully coherent TB [18]. Note that the Zn/Y atoms are at ABAB stacking sequence in the twin. This agrees well with reorientation of the SFs enriched with Zn/Y atoms during twinning at 300 °C [13]. It should be mentioned here that the stacking sequence of Zn/Y atoms is the key feature to distinguish the matrix (AB′C′A) and twin (ABAB) in this kind of Mg alloys. This clarified that the matrix and twin could be uniquely distinguished. From a deformation mechanism point of view, the solute atoms (Zn and Y) can be used to probe the progress of matrix into deformation twin. Fig. 8d demonstrates the atomic steps in the original segments of SFs, with 2–6 basal planes height (marked by arrows), associated with dislocations with *c* Burgers vector, as shown by "T". This implies that non-basal dislocations were activated in the Mg-Zn-Y alloys during deformation at room temperature, which was due to the increase of activation energy of basal dislocations [14].

4. Discussion

4.1. Mechanisms of segregation of solute atoms at the KBs

As demonstrated above, the solute atoms in Mg-Zn-Y alloy may be in a random distribution, form nanoscale clusters or be in a periodic pattern along symmetrical deformation-induced KB, as shown in Figs. 3 and 4. This strongly suggests that solute atoms prefer to segregate along these KBs upon deformation, in combination with the KBs in LPSO structures associated with bright contrast [41]. The symmetrical boundaries, like GBs [46,47] and TBs [18] in metallic materials and ceramics and so on, have been reported to be segregated with solute atoms. This is driven by the minimization of free energy according to the Gibbs adsorption isotherm, as it should do in the current case of the segregation of solute atoms to the symmetrical KB in this Mg alloy.

The symmetrical KBs are proved to be Zn enriched in LPSO phase/SFs and in adjacent Mg layers, and a few Y atoms concentrated in KB of LPSO structure, as is evident in Figs. 5 and 6. The corresponding atomic mechanisms here qualitatively responsible for the apparent segregation of Zn atoms to KB were proposed as follows. Firstly, the anisotropic diffusivity of impurity in Mg was reported, and it is 1.23 times higher along a-axis than along c-axis [48]. The diffusion coefficient of Zn is about one order of magnitude higher than that of Y and self-diffusion of Mg [49]. The temperature-dependent diffusion coefficients of Zn and Y along a-axis and c-axis are $D^{Zn/Y}_{a/c-axis} = D_o \times \exp(-Q/RT)$, where R is the gas constant and T is the absolute temperature [48,49]. The pre-

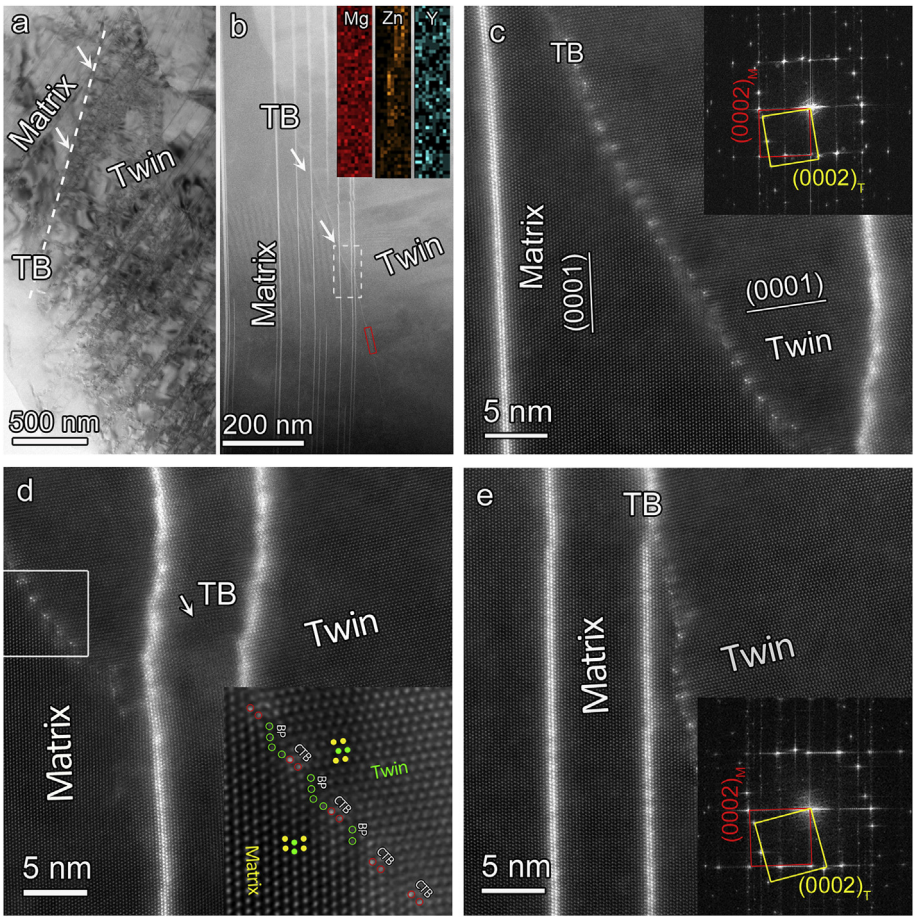

Fig. 7. (a) A bright-field TEM image of {10$\bar{1}$ 2} deviated deformation twin. (b) Corresponding STEM image of the {10$\bar{1}$ 2} twin. The inserted EDS analysis of the TB framed by red rectangle implies that Zn atoms segregate to TBs. (c) Atomic resolution STEM image of the area framed in (b) demonstrating the interaction between TB and SFs. The inset FFT pattern indicates that the twin angle is about 95.9°. Note that the periodic segregation of Zn/Y atoms occurs along the TB. (d) The above periodic segregation of Zn/Y atoms does not occur in a particular section of the TB. Note that such a section is within a pair of SFs, 8 nm apart from each other. The inset in (d) is a high-resolution STEM image showing a combination of TB and BPs. The coherent segment of {10$\bar{1}$ 2} TB is segregated with Zn/Y atoms (circled in red); while the BPs is free of Zn/Y atoms segregations (circled in green). (e) High-resolution STEM image showing a random distribution of solute atoms along the TB. Such a disorder is a resultant from the interaction of TB with two units of SFs. The inset is an FFT pattern showing the misorientation of basal plane of matrix and that of twin is approximately 102.5°. (For interpretation of the references to colour in this figure legend, the reader is referred to the web version of this article.)

exponential factor *Do* and activation energy *Q* are listed in Table 2. This could explain that the GB segregation of Mg alloys after hot deformation or homogenization [16,17]. However, the diffusion coefficients of Zn and Y atoms at room temperature were calculated to be so small (in the order of 10^{-28} m^2s^{-1}) that diffusion of Zn/Y is ruled out here. The Zn/Y lattice diffusion thus may contribute little to the significant segregation along KB at room temperature. Secondly, the KB is formed by the synchronized movement of 1/3<11$\bar{2}$ 0> basal dislocations in LPSO structures [5]. The partial dislocations sweeping the basal plane of LPSO structure may destabilize the LPSO structures, since movement of partial dislocations within an intermetallic compound has been reported to result in a local composition deviation from its stoichiometric ratio [50,51]. Moreover, the shuffling Zn/Y atoms may diffuse along basal dislocations in LPSO structures, for the dislocations can transport atoms at rates orders of magnitude faster than bulk diffusion in a crystal [52]. The dislocation-enhanced diffusion hence should be responsible for segregation of KB in LPSO structures or SFs upon deformation at room temperature. Thirdly, the KB which accommodated dislocation arrays may serve as a very local faster path for the transfer of solute atoms into the sandwiched Mg layers. Here the KB is analogous to the grain boundary, which is often imagined to be a sort of short circuit path of high diffusivity. This led to the enrichment of solute atoms along KB from LPSO structures/SFs into sandwiched Mg layers. It's still not well understood why fast diffusion of Zn atoms along dislocations compared to Y atoms yet at this stage; nevertheless, considering the size difference between Y and Mg atoms, the diffusivity is expected to be low.

The segregation of solute atoms at KB is about 2 nm in width, as shown in Figs. 3–6. This is in line with the range of Cottrell atmospheres around dislocations, ~1.5–3 nm in diameter, which was an upper limit of the radial extent of impurities via atom probe tomography [53,54]. Further, it is worth mentioning that Zn atoms along KB in LPSO were approximately 1.5 times more than those along KB in SF (Table 1), which may indicate that the stacking and chemical ordered structure of LPSO phase may effectively decrease the diffusion rate of solute atoms along KB longitudinally from LPSO into Mg layers.

4.2. Proposed process of segregation at KBs

The process of solute segregation during deformation kink is schematically illustrated in Fig. 9. The unique intergrowth microstructure of LPSO structures and Mg layers formed in the Mg-Zn-Y alloys (Fig. 9a), where the basal plane of Mg and LPSO structures is parallel to each other. Basal dislocations are activated to

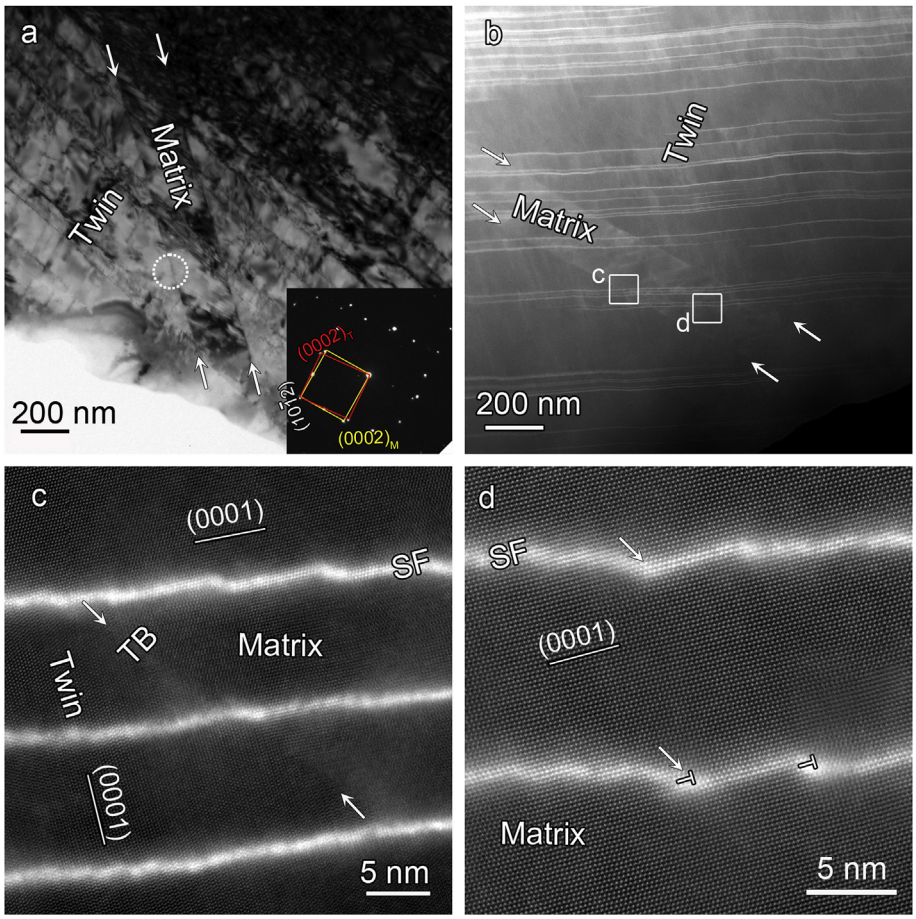

Fig. 8. (a) A bright-filed TEM image of the microstructure of matrix and a {10$\bar{1}$ 2} deformation twin. The inset is a selected area electron diffraction (SAED) pattern of the twin. (b) A low magnification HAADF-STEM image corresponding to (a), with a small anti-clockwise rotation. Clearly, profuse rumpled stacking faults enriched with Zn/Y, as shown as horizontal bright lines, are continuous in between matrix and twin. (c) A high magnification HAADF-STEM image of the area marked with square *c* in (b), suggesting the overlapped TBs are free of Zn/Y segregation. (d) A high magnification STEM image of the area marked with square *d* in (b), demonstrating that the SFs in the matrix are sheared after deformation.

Table 2
The list of pre-exponential factors and activation energy of Zn and Y atoms in HCP Mg alloys [48,49].

	Pre-exponential factor Do	Activation energy Q (KJ/mol)	Ref
D^{Zn}_{a-axis}	4.98×10^{-5}	132.725	[48]
D^{Zn}_{c-axis}	7.33×10^{-5}	135.488	
D^{Y}_{a-axis}	2.79×10^{-8}	97.852	[49]
D^{Y}_{c-axis}	3.21×10^{-8}	99.127	

accommodate the local strain both in two phases upon deformation, as shown in Fig. 9b. Simultaneously, Zn atoms are proposed to diffuse and segregate to KB owing to the defect-enhanced diffusion, leading to the local solute supersaturation at the KB of LPSO structures. This would accelerate the atoms transfer from the Zn/Y planes into Mg planes, and then from LPSO phase/SFs into Mg layers. Fig. 9c shows the distribution of atoms at KB and the diffusion directions along KB. Of course, a few of Zn atoms distributing in Mg matrix diffuse into the KB of Mg interlayers along basal planes should be also taken into account, due to approximately 0.03 at.% Zn atoms in the Mg interlayers. Zn atoms in the KBs are thus proposed to be from both LPSO structures and Mg interlayers.

The local decomposition induced by plastic deformation has been experimentally observed and simulated in Al alloys [50,51], some steels [55] and Al-Mg alloys [56,57], which were rationalized based on the interaction of solute atoms and dislocation movement or deformation induced vacancies. As demonstrated and discussed above, the amount of solute atoms at KB is 2–3 times of that in LPSO structures or SFs. This means that the local composition along KB is significantly deviated from the stoichiometric ratio, which was owing to the dislocation motion upon deformation. Therefore, it undoubtedly proved that plastic deformation led to the redistribution of solute atoms through the fast diffusion of Zn atoms along basal planes and KBs, as well as the subsequent local decomposition of LPSO phase/SFs near KB in Mg alloys.

4.3. Solute atoms at the various TBs

In HCP metals, strain along the c-axis could be accommodated by twining or <***c*** + ***a***> dislocations [58]. Although the LPSO phase could partially block the propagation of deformation twins [5,9], we actually observed a few deformation twins in our Mg-Zn-Y alloys compressed at room temperature. The coherent segments of {10$\bar{1}$ 2} TBs are segregated with Zn atoms and no detectable Y atoms, as shown in Fig. 7. This is consistent with the results reported by Nie et al. [18]. They reported that {10$\bar{1}$ 1}, {10$\bar{1}$ 2} and {10$\bar{1}$ 3} coherent TBs are periodically segregated with Zn or Gd in dilute Mg alloys after annealing for several minutes. The segregation of solute atoms to the coherent segments of TB may be driven by the minimization of total energy and elastic strain energy in the

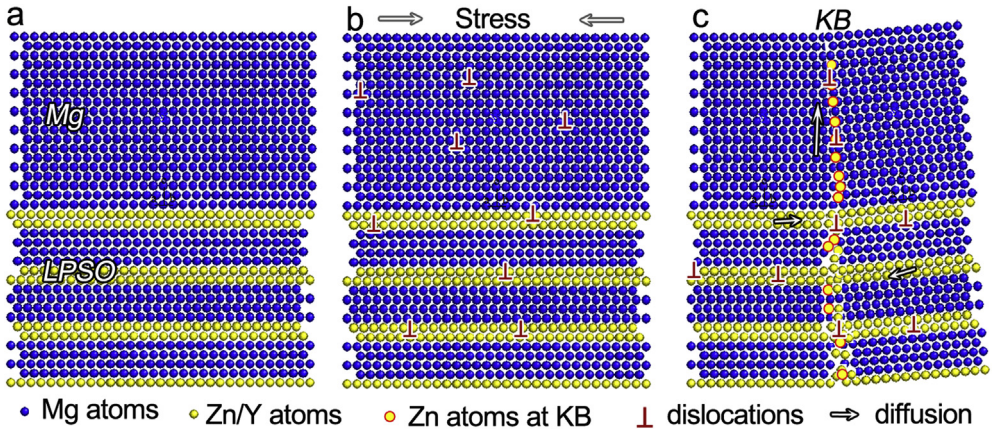

Fig. 9. Schematic illustration of the dislocation-enhanced diffusion of Zn (circled in red) towards KBs and then transmission along KB. (a) The original sandwiched microstructure containing LPSO phases and Mg layers. (b) Basal dislocations are activated both in LPSO structure and Mg layers upon load, resulting in the diffusion of solute atoms. (c) Zn atoms preferentially segregate to the deformation-induced KB, promoted by the basal dislocations and dislocation arrays along the KB. (For interpretation of the references to colour in this figure legend, the reader is referred to the web version of this article.)

system, which was proposed by Nie et al. to rationalize that Zn and RE elements orderly segregate to the twin boundaries based on *ab* initio simulation [18].

However, the $\{10\bar{1}\ 2\}$ overlapped TBs between SFs were free of Zn/Y atoms. This may be closely related to the lattice overlap of matrix and twin along the recorded direction, as denoted by arrows in Figs. 7d and 8c. In detail, the blurry TBs are due to the strong interaction between lamellar LPSO structure/SFs and the deformation twins [13]. Shockley partials associated to the lamellar LPSO structures would redirect the twin dislocation into the directions other than $<10\bar{1}\ 1>$, leading to no edge-on structure when viewed parallel to $<11\bar{2}\ 0>$ zone axis. Last but not least, few solute atoms distributing in matrix between SFs apart from each other smaller than 10 nm, since a large proportion of solute atoms concentrated in SFs during cast process. Thus, no supersaturated atoms could segregate to deformation TB. Combined with the TBs decorated with Zn atoms, we may conclude that the segregation to the TBs is closely related to the boundaries configuration and the solute contents in the matrix.

5. Conclusions

By means of aberration-corrected scanning transmission electron microscopy, we provide the atomic-scale mapping of the solute atoms segregation at the deformation-induced symmetrical boundaries in an Mg-Zn-Y alloy. We draw the following conclusions:

1. The solute atoms segregation occurs at the symmetrical KBs in LPSO structures/SFs and sandwiched Mg layers in Mg-Zn-Y alloy. These enriched atoms may be in a random fashion, form nanoscale clusters or in a periodic pattern along $<11\bar{2}\ 0>$ zone axis. The unique configuration of segregated solute atoms here is closely related to the local microstructure of KB.
2. Zn atoms obviously segregate to KBs both in LPSO structures and Mg layers, while only a small amount of Y atoms could be detected at KB in LPSO structure. The content of Zn atoms concentrated at KBs in LPSO structures and SFs is approximately 3 and 2 times of that in LPSO structures and SFs, respectively. The solute segregation along KBs in Mg alloy is proposed to result from dislocation-enhanced diffusion.
3. The coherent segments of $\{10\bar{1}\ 2\}$ TBs is orderly decorated with Zn atoms but no discerned Y atoms during deformation. In contrast, the overlapped TBs in between lamellar LPSO phases/SFs were free of solute atoms. The segregation of solute atoms at TBs highly depends on the atomic structure of TBs and the amount of solute atoms in the local region.

Acknowledgements

This work is supported by the National Natural Science Foundation of China (grants 51301177), the National Basic Research Program of China (grants 2014CB921002), the Innovation Fund of IMR (SCJJ-2013-PY-08 & 2015-PY08), and the Fund of SYNL (2015FP18). The authors at SYNL are grateful to B. Wu and L. X. Yang of this laboratory for their technical support on the Titan platform of the aberration-corrected scanning transmission electron microscope.

References

[1] A. Inoue, Y. Kawamura, M. Matsushita, K. Hayashi, J. Koike, Novel hexagonal structure and ultrahigh strength of magnesium solid solution in the Mg-Zn-Y system, J. Mater. Res. 16 (2001) 1894–1900.
[2] Y. Kawamura, K. Hayashi, A. Inoue, T. Masumoto, Rapidly solidified powder metallurgy $Mg_{97}Zn_1Y_2$ alloys with excellent tensile yield strength above 600 MPa, Mater. Trans. 42 (2001) 1172–1176.
[3] S. Yoshimoto, M. Yamasaki, Y. Kawamura, Microstructure and mechanical properties of extruded Mg-Zn-Y alloys with 14H long period ordered structure, Mater. Trans. 47 (2006) 959–965.
[4] K. Hagihara, A. Kinoshita, Y. Sugino, M. Yamasaki, Y. Kawamura, H.Y. Yasuda, Y. Umakoshi, Effect of long-period stacking ordered phase on mechanical properties of $Mg_{97}Zn_1Y_2$ extruded alloy, Acta Mater. 58 (2010) 6282–6293.
[5] X.H. Shao, Z.Q. Yang, X.L. Ma, Strengthening and toughening mechanisms in Mg-Zn-Y alloy with a long period stacking ordered structure, Acta Mater. 58 (2010) 4760–4771.
[6] K. Hagihara, A. Kinoshita, Y. Sugino, M. Yamasaki, Y. Kawamura, H. Yasuda, Y. Umakoshi, Plastic deformation behavior of $Mg_{89}Zn_4Y_7$ extruded alloy composed of long-period stacking ordered phase, Intermetallics 18 (2010) 1079–1085.
[7] K. Hagihara, N. Yokotani, Y. Umakoshi, Plastic deformation behavior of $Mg_{12}YZn$ with 18R long-period stacking ordered structure, Intermetallics 18 (2010) 267–276.
[8] E. Oñorbe, G. Garcés, P. Perez, P. Adeva, Effect of the LPSO volume fraction on the microstructure and mechanical properties of Mg-Y_{2X} -Zn_X alloys, J. Mater. Sci. 47 (2012) 1085–1093.
[9] M. Matsuda, S. Ii, Y. Kawamura, Y. Ikuhara, M. Nishida, Interaction between long period stacking order phase and deformation twin in rapidly solidified $Mg_{97}Zn_1Y_2$ alloy, Mat. Sci. Eng. A-struct 386 (2004) 447–452.
[10] M. Matsuda, S. Ando, M. Nishida, Dislocation structure in rapidly solidified Mg97Zn1Y2 alloy with long period stacking order phase, Mater. Trans. 46 (2005) 361–364.
[11] M. Yamasaki, T. Anan, S. Yoshimoto, Y. Kawamura, Mechanical properties of warm-extruded Mg-Zn-Gd alloy with coherent 14H long periodic stacking

ordered structure precipitate, Scr. Mater. 53 (2005) 799–803.
[12] G. Garcés, M. Maeso, I. Todd, P. Pérez, P. Adeva, Deformation behaviour in rapidly solidified $Mg_{97}Y_2Zn_1$ (at.%) alloy, J. Alloy. Compd. 432 (2007) L10–L14.
[13] X.H. Shao, Z.Q. Yang, X.L. Ma, Interplay between deformation twins and basal stacking faults enriched with Zn/Y in $Mg_{97}Zn_1Y_2$ alloy, Phil. Mag. Lett. 94 (2014) 150–156.
[14] J.-K. Kim, S. Sandlöbes, D. Raabe, On the room temperature deformation mechanisms of a Mg–Y–Zn alloy with long-period-stacking-ordered structures, Acta Mater. 82 (2015) 414–423.
[15] T. Itoi, K. Takahashi, H. Moriyama, M. Hirohashi, A high-strength Mg–Ni–Y alloy sheet with a long-period ordered phase prepared by hot-rolling, Scr. Mater. 59 (2008) 1155–1158.
[16] M. Bugnet, A. Kula, M. Niewczas, G.A. Botton, Segregation and clustering of solutes at grain boundaries in Mg–rare earth solid solutions, Acta Mater. 79 (2014) 66–73.
[17] J.P. Hadorn, T.T. Sasaki, T. Nakata, T. Ohkubo, S. Kamado, K. Hono, Solute clustering and grain boundary segregation in extruded dilute Mg–Gd alloys, Scr. Mater. 93 (2014) 28–31.
[18] J.F. Nie, Y.M. Zhu, J.Z. Liu, X.Y. Fang, Periodic segregation of solute atoms in fully coherent twin boundaries, Science 340 (2013) 957–960.
[19] Z. Yang, M.F. Chisholm, G. Duscher, X. Ma, S.J. Pennycook, Direct observation of dislocation dissociation and Suzuki segregation in a Mg–Zn–Y alloy by aberration-corrected scanning transmission electron microscopy, Acta Mater. 61 (2013) 350–359.
[20] P.R. Cantwell, M. Tang, S.J. Dillon, J. Luo, G.S. Rohrer, M.P. Harmer, Grain boundary complexions, Acta Mater. 62 (2014) 1–48.
[21] T. Chookajorn, H.A. Murdoch, C.A. Schuh, Design of stable nanocrystalline alloys, Science 337 (2012) 951–954.
[22] M. Kuzmina, D. Ponge, D. Raabe, Grain boundary segregation engineering and austenite reversion turn embrittlement into toughness: example of a 9wt.% medium Mn steel, Acta Mater. 86 (2015) 182–192.
[23] M. Koyama, E. Akiyama, T. Sawaguchi, D. Raabe, K. Tsuzaki, Hydrogen-induced cracking at grain and twin boundaries in an Fe-Mn-C austenitic steel, Scr. Mater. 66 (2012) 459–462.
[24] N. Shibata, M.F. Chisholm, A. Nakamura, S.J. Pennycook, T. Yamamoto, Y. Ikuhara, Nonstoichiometric dislocation cores in alpha-alumina, Science 316 (2007) 82–85.
[25] Z.C. Wang, M. Saito, K.P. McKenna, L. Gu, S. Tsukimoto, A.L. Shluger, Y. Ikuhara, Atom-resolved imaging of ordered defect superstructures at individual grain boundaries, Nature 479 (2011) 380–383.
[26] B.B. Sun, Y.B. Wang, J. Wen, H. Yang, M.L. Sui, J.Q. Wang, E. Ma, Artifacts induced in metallic glasses during TEM sample preparation, Scr. Mater. 53 (2005) 805–809.
[27] D.J. Barber, Radiation-damage in ion-milled specimens - characteristics, effects and methods of damage limitation, Ultramicroscopy 52 (1993) 101–125.
[28] E. Abe, Y. Kawamura, K. Hayashi, A. Inoue, Long-period ordered structure in a high-strength nanocrystalline Mg-1 at% Zn-2 at% Y alloy studied by atomic-resolution Z-contrast STEM, Acta Mater. 50 (2002) 3845–3857.
[29] Y.M. Zhu, A.J. Morton, J.F. Nie, The 18R and 14H long-period stacking ordered structures in Mg-Y-Zn alloys, Acta Mater. 58 (2010) 2936–2947.
[30] X.H. Shao, H.J. Yang, J.T.M. De Hosson, X.L. Ma, Microstructural characterization of long-period stacking ordered phases in $Mg_{97}Zn_1Y_2$ (at.%) alloy, Microsc. Microanal. 19 (2013) 1575–1580.
[31] K. Kishida, K. Nagai, A. Matsumoto, A. Yasuhara, H. Inui, Crystal structures of highly-ordered long-period stacking-ordered phases with 18R, 14H and 10H-type stacking sequences in the Mg–Zn–Y system, Acta Mater. 99 (2015) 228–239.
[32] M. Yamasaki, M. Matsushita, K. Hagihara, H. Izuno, E. Abe, Y. Kawamura, Highly-ordered 10*H*-type long-period stacking order phase in a Mg-Zn-Y ternary alloy, Scr. Mater. 78–79 (2014) 13–16.
[33] K. Kishida, H. Yokobayashi, H. Inui, M. Yamasaki, Y. Kawamura, The crystal structure of the LPSO phase of the 14H-type in the Mg–Al–Gd alloy system, Intermetallics 31 (2012) 55–64.
[34] K. Kishida, H. Yokobayashi, H. Inui, The most stable crystal structure and the formation processes of an order-disorder (OD) intermetallic phase in the Mg–Al–Gd ternary system, Phil. Mag. 93 (2013) 2826–2846.
[35] D.H. Ping, K. Hono, Y. Kawamura, A. Inoue, Local chemistry of a nanocrystalline high-strength $Mg_{97}Y_2Zn_1$ alloy, Phil. Mag. Lett. 82 (2002) 543–551.
[36] J.F. Nie, K. Oh-ishi, X. Gao, K. Hono, Solute segregation and precipitation in a creep-resistant Mg-Gd-Zn alloy, Acta Mater. 56 (2008) 6061–6076.
[37] J.F. Nie, Precipitation and hardening in magnesium alloys, Metall. Mater. Trans. a-Phys. Metall. Mater. Sci. 43A (2012) 3891–3939.
[38] M. Yamasaki, K. Hagihara, S.-i. Inoue, J.P. Hadorn, Y. Kawamura, Crystallographic classification of kink bands in an extruded Mg–Zn–Y alloy using intragranular misorientation axis analysis, Acta Mater. 61 (2013) 2065–2076.
[39] S. Pennycook, D. Jesson, High-resolution incoherent imaging of crystals, Phys. Rev. Lett. 64 (1990) 938–941.
[40] S.J. Pennycook, Structure determination through Z-contrast microscopy, Adv. Imaging Electron Phys. 123 (2002) 173–206.
[41] J.F. Nie, Y.M. Zhu, A.J. Morton, On the structure, transformation and deformation of long-period stacking ordered phases in Mg-Y-Zn alloys, Metall. Mater. Trans. a-Phys. Metall. Mater. Sci. 45A (2014) 3338–3348.
[42] G. Sha, K. Tugcu, X.Z. Liao, P.W. Trimby, M.Y. Murashkin, R.Z. Valiev, S.P. Ringer, Strength, grain refinement and solute nanostructures of an Al–Mg–Si alloy (AA6060) processed by high-pressure torsion, Acta Mater. 63 (2014) 169–179.
[43] X.Y. Zhang, B. Li, X.L. Wu, Y.T. Zhu, Q. Ma, Q. Liu, P.T. Wang, M.F. Horstemeyer, Twin boundaries showing very large deviations from the twinning plane, Scr. Mater. 67 (2012) 862–865.
[44] J. Tu, X.Y. Zhang, C. Lou, Q. Liu, HREM investigation of twin boundary and interface defects in deformed polycrystalline cobalt, Phil. Mag. Lett. 93 (2013) 292–298.
[45] J. Tu, X.Y. Zhang, J. Wang, Q. Sun, Q. Liu, C.N. Tome, Structural characterization of {10(1)over-bar2} twin boundaries in cobalt, Appl. Phys. Lett. 103 (2013), 051903(051901-051904).
[46] J.P. Buban, K. Matsunaga, J. Chen, N. Shibata, W.Y. Ching, T. Yamamoto, Y. Ikuhara, Grain boundary strengthening in alumina by rare earth impurities, Science 311 (2006) 212–215.
[47] C.M. Barr, G.A. Vetterick, K.A. Unocic, K. Hattar, X.M. Bai, M.L. Taheri, Anisotropic radiation-induced segregation in 316L austenitic stainless steel with grain boundary character, Acta Mater. 67 (2014) 145–155.
[48] S.K. Das, Y.M. Kim, T.K. Ha, I.H. Jung, Investigation of anisotropic diffusion behavior of Zn in hcp Mg and interdiffusion coefficients of intermediate phases in the Mg-Zn system, Calphad 42 (2013) 51–58.
[49] S.K. Das, Y.-B. Kang, T. Ha, I.-H. Jung, Thermodynamic modeling and diffusion kinetic experiments of binary Mg–Gd and Mg–Y systems, Acta Mater. 71 (2014) 164–175.
[50] D. Chen, X.L. Ma, Local decomposition induced by dislocation motions inside tetragonal Al2Cu compound: slip system-dependent dynamics, Sci. Rep. 3 (2013) 3157, http://dx.doi.org/10.1038/srep03157.
[51] B. Yang, Y.T. Zhou, D. Chen, X.L. Ma, Local decomposition induced by dislocation motions inside precipitates in an Al-alloy, Sci. Rep. 3 (2013) 1039, http://dx.doi.org/10.1038/srep01039.
[52] M. Legros, G. Dehm, E. Arzt, T.J. Balk, Observation of giant diffusivity along dislocation cores, Science 319 (2008) 1646–1649.
[53] D. Blavette, E. Cadel, A. Fraczkiewicz, A. Menand, Three-dimensional atomic-scale imaging of impurity segregation to line defects, Science 286 (1999) 2317–2319.
[54] K. Thompson, P.L. Flaitz, P. Ronsheim, D.J. Larson, T.F. Kelly, Imaging of arsenic Cottrell atmospheres around silicon defects by three-dimensional atom probe tomography, Science 317 (2007) 1370–1374.
[55] L. Zhou, G. Liu, X.L. Ma, K. Lu, Strain-induced refinement in a steel with spheroidal cementite subjected to surface mechanical attrition treatment, Acta Mater. 56 (2008) 78–87.
[56] X. Sauvage, A. Ganeev, Y. Ivanisenko, N. Enikeev, M. Murashkin, R. Valiev, Grain boundary segregation in UFG alloys processed by severe plastic deformation, Adv. Eng. Mater. 14 (2012) 968–974.
[57] X. Sauvage, N. Enikeev, R. Valiev, Y. Nasedkina, M. Murashkin, Atomic-scale analysis of the segregation and precipitation mechanisms in a severely deformed Al–Mg alloy, Acta Mater. 72 (2014) 125–136.
[58] M.H. Yoo, Slip, twinning, and fracture in hexagonal close-packed metals, Metall. Trans. A 12 (1981) 409–418.